

Conserved quantities enable the quantum Mpemba effect in weakly open systems

Iris Ulčakar,^{1,2} Gianluca Lagnese,¹ Rustem Sharipov,² and Zala Lenarčič¹

¹Jožef Stefan Institute, 1000 Ljubljana, Slovenia

²University of Ljubljana, Faculty for physics and mathematics, 1000 Ljubljana, Slovenia

Observation of the quantum Mpemba effect has spurred much interest in its enabling conditions and its relation to the classical counterpart. Here, we consider weakly open many-body quantum systems initialized in different thermal states and examine when the initially farther state relaxes to the (non-equilibrium) steady state faster. We claim that the number of conserved quantities in the unitary part plays a crucial role: the Mpemba effect is possible only when the Hamiltonian commutes with other extensive operators or is integrable. The reason lies in the dynamical evolution happening in spaces of different dimensions. When energy is the only approximately conserved quantity, dissipation pushes the dynamics within a single-parameter manifold of different thermal states. In contrast, for Hamiltonians with several conserved quantities, the dynamics drift in the multi-dimensional space of generalized Gibbs ensembles, whose distance to the steady state is less trivial. We provide numerical results for large system sizes using tensor networks and free-fermion techniques, thereby supporting our claim.

The Mpemba effect is the counter-intuitive phenomenon where, under certain conditions, a hotter system cools faster than a colder one. Its occurrence challenges the conventional thermodynamic intuition and, since its popularization in the 1989 [1], sparked numerous debates and scientific investigations [2–23] without an universally accepted explanation of the original experiment [24, 25]. Recent research revealed quantum analogs of the Mpemba effect [26], which can be divided into two classes: isolated and open quantum systems.

In closed quantum systems, the effect was first observed in processes of symmetry restoration in integrable Hamiltonian models. The system is prepared in different pure states that violate a symmetry of the Hamiltonian to a different degree, and the effect is naturally detected by monitoring a suitable quantification of the asymmetry during the time evolution after a quench [27–30]. The phenomenon was also confirmed experimentally with trapped ions [31]. Furthermore, based on the quasi-particle picture [32–34] allowed by the integrable structure, a microscopic interpretation was proposed [35]. Subsequently, the analysis has been extended to a broader class of systems such as quantum circuits [36–43], many-body localized systems [44], two-dimensional systems of free bosons and free fermions [45, 46], and chaotic systems without any conserved quantities [47]. As a more generally applicable measure, a comparison was introduced between the reduced density matrix of a subsystem and its steady-state equivalent.

The second type of models that can exhibit the quantum Mpemba effect are open (driven) quantum systems, where the system interacts with an environment. Strategies to realize the Mpemba effect include: (i) orthogonalization of the initial state with respect to the slowest decaying mode [48–62]; (ii) few-body systems of qubit(s), quantum dots, or harmonic oscillator coupled to thermal baths [52–61, 63–70]; (iii) a cooling protocol in a system with a metastable configuration due to a first-order

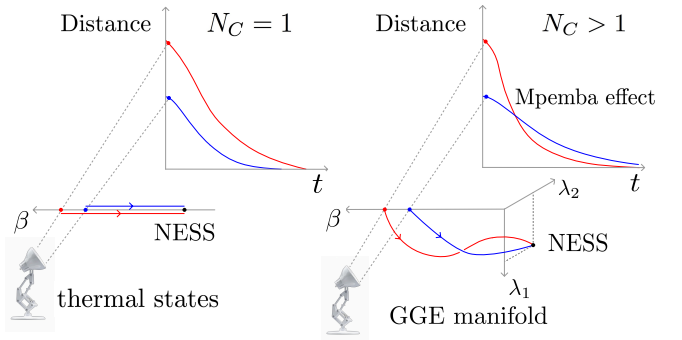


FIG. 1. We consider many-body quantum systems with unitary Hamiltonian and a weak dissipative evolution, initialized in two thermal states. $N_C = 1$: For Hamiltonians without additional conserved quantities, each dynamics can be approximated by a thermal ensemble with a time-dependent temperature. $N_C > 1$: For Hamiltonians with more conserved quantities, dissipation can steer the evolution from thermal states in the multi-dimensional manifold of generalized Gibbs ensembles (GGEs). When projecting the dynamics onto a scalar - the distance between the time-evolved and the non-equilibrium steady state (NESS) - crossings can happen in the presence of multiple approximately conserved quantities.

phase transition [71] and a supercooling protocol with a strong coupling to a thermal bath [72]; and (iv) proposals for quantum-optical implementations employing different initial states of light [73, 74]. Some of these strategies have classical Markovian analogues, such as the orthogonalization procedure [12–15] and supercooling protocols [75, 76]. Stability of symmetry restoration has also been tested with respect to the presence of dissipation [31, 77].

In this Letter, we provide a general and unifying principle for the occurrence of the Mpemba effect in thermodynamically large weakly open systems, based on the local symmetries of the Hamiltonian. In resemblance to the classical setup, we discuss systems initialized in mixed

thermal states, thus not pursuing effects due to fine tuned coherence of the initial state. We propagate the density matrix with a unitary Hamiltonian evolution in the presence of weak coupling to nonequilibrium Lindblad baths and ask how the occurrence of the Mpemba effect — a farther state relaxing to the steady state faster than a closer one — depends on the generic properties of the many-body Hamiltonian. We claim that the number of conserved quantities of the underlying Hamiltonian, being weakly broken by the dissipation, is crucial. We give evidence that chaotic many-body models with Hamiltonian as the only approximate conserved quantity cannot exhibit the Mpemba effect, while systems with additional approximate conserved quantities — integrable Hamiltonians being the extreme case — allow for it. Using tensor network and free fermions approaches, we provide large system sizes $80 \geq L \geq 400$ results supporting our claim.

Setup. We consider weakly dissipative quantum many-body systems with a dominant unitary evolution. Weak dissipation is encoded in bulk Lindblad operators L_j acting around every site j at a rate $\epsilon \ll 1$,

$$\dot{\rho} = -i[H, \rho] + \hat{D}\rho, \quad \hat{D}\rho = \epsilon \sum_j L_j \rho L_j^\dagger - \frac{1}{2} \{L_j^\dagger L_j, \rho\}. \quad (1)$$

In the weak-dissipation regime, the density matrix describing the system can be decomposed as [78]

$$\rho(t) = \rho_\lambda(t) + \delta\rho(\epsilon, t), \quad (2)$$

where $\rho_\lambda(t)$ is a dominant component independent of ϵ and $\delta\rho(\epsilon, t)$ is small correction. The conserved quantities C_i of the unitary part, $[H, C_i] = 0$, play an important role in the parametrization $\lambda = \{\lambda_i\}_{i=1}^{N_C}$ of the zeroth order approximation $\rho_\lambda(t)$. Namely, one can use a statistical description by introducing a Lagrange parameter λ_i for each approximately conserved quantity [79–96],

$$\rho_\lambda(t) = \frac{e^{-\sum_{i=1}^{N_C} \lambda_i(t) C_i}}{\text{Tr}[e^{-\sum_{i=1}^{N_C} \lambda_i(t) C_i}].} \quad (3)$$

When the Hamiltonian is the only approximate conserved quantity ($N_C = 1$), $\rho_\lambda(t)$ takes the form of a time dependent Gibbs ensemble $\rho_\beta(t) = e^{-\beta(t)H}/\text{Tr}[e^{-\beta(t)H}]$, parametrized with a time dependent inverse temperature [79–81]. In the presence of additional symmetries, e.g., for a weakly open integrable evolution, $\rho_\lambda(t)$ takes the form of a time dependent generalized Gibbs ensemble (GGE) parametrized with $N_C > 1$ Lagrange parameters [82–96]. Due to the weak coupling to baths, energy and other conserved quantities are only approximately conserved and are slowly changing due to the dissipation, $\langle \dot{C}_i \rangle = \text{Tr}[C_i \hat{D}\rho(t)] \approx \text{Tr}[C_i \hat{D}\rho_\lambda(t)]$. Equivalently, the dissipator super-operator governs the time evolution of the temperature and other Lagrange parameters [83],

$$\dot{\lambda}_i(t) = - \sum_{i'=1}^{N_C} \chi_{ii'}^{-1}(t) \text{Tr}[C_{i'} \hat{D}\rho_\lambda(t)], \quad (4)$$

where $\chi_{ii'}(t) = \text{Tr}[C_i C_{i'} \rho_\lambda(t)] - \text{Tr}[C_i \rho_\lambda(t)] \text{Tr}[C_{i'} \rho_\lambda(t)]$.

Methods. Without assuming any perturbative expansion in small ϵ , time evolution of density matrices $\rho(t)$ are obtained by performing a tensor-network (TN) simulation of the Lindblad equation Eq. (1) with open boundary conditions. We employ 4th order time-evolving block decimation for the vectorized density matrix [97] on system sizes $80 \leq L \leq 160$, using bond dimension $160 \leq \chi \leq 240$ and time step $0.05 \leq dt \leq 0.2$. In the weak-coupling limit, the G(GE) approximation to the density matrix Eq. (3) is obtained by evaluating Eq. (4). For the chaotic Hamiltonian without other conserved quantities, Eq. (4) reduces to an equation of motion for the inverse temperature $\dot{\beta}(t) = f(\beta(t))$. We compute this on $L = 80$ sites using a tensor-network representation, with thermal states $\rho_\beta(t)$ obtained via imaginary-time evolution [98]. For the integrable case, we consider a non-interacting Hamiltonian H , for which Eq. (4) can be evaluated in thermodynamically large systems by working in the free-fermion representation. As noted in Ref. [87] and the Supplementary Material, $\rho_\lambda(t)$ is then parametrized by time-dependent chemical potentials, which act as Lagrange parameters for the nearly conserved quasiparticle occupations. Their time dependence is calculated from the scattering equation, derived in Ref. [87] and in the Supplementary Material, capturing scattering/creation/annihilation of quasiparticles due to the Lindblad perturbation. In the fermionic formulation we employ periodic boundary conditions. However, since our Lindblad operators do not induce currents, the choice of boundary conditions is not essential for sufficiently large system sizes.

We detect the quantum Mpemba effect by comparing distances between time-evolved states $\rho(t)$ and the steady state ρ_∞ . This can be done either for the full density matrix or the zeroth order (G)GE obtained as described above. The Mpemba effect manifests itself when a state initialized farther from the steady state approaches it faster than one initialized closer. There is some debate regarding which definition of distance should be used [26]. While the trace distance, $\text{Tr}[\sqrt{(\rho(t) - \rho_\infty)^2}]$, might formally be the most appropriate, it is not suitable for calculations with tensor networks. We employ here a normalized Frobenius norm, evaluated on reduced density matrices of a subsystem A (chosen in the middle of the system) of compact support $\ell = |A|$,

$$d_\ell(\rho(t), \rho_\infty) = \sqrt{\frac{\text{Tr}[(\rho_A(t) - \rho_{\infty,A})^2]}{\text{Tr}[(\rho_A(t))^2] + \text{Tr}[(\rho_{\infty,A})^2]}}, \quad (5)$$

where we introduce the notation $\rho_A(t) = \text{Tr}_{\bar{A}}[\rho(t)]$ and $\rho_{\infty,A} = \text{Tr}_{\bar{A}}[\rho_\infty]$. This norm can be readily implemented within the matrix product state representation of $\rho(t)$ and thermal states $\rho_\beta(t)$. It is likewise straightforward to compute in the free-fermion Gaussian representation of the GGE $\rho_\lambda(t)$, where the correlation matrix is employed

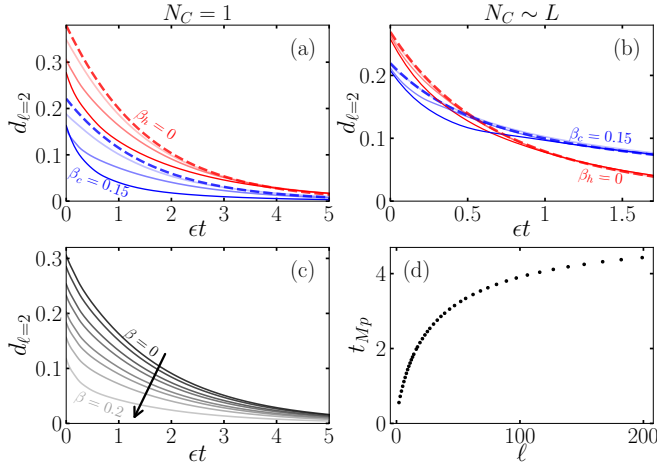


FIG. 2. (a,b) Distances $d_{\ell=2}(\rho(t), \rho_\infty)$ as a function of rescaled time et for the initial thermal states with $\beta_c = 0.15$ (blue) and $\beta_h = 0$ (red) inverse temperature for (a) chaotic and (b) integrable transverse field Ising Hamiltonian H . Results for $\epsilon = 0.05, 0.2, 0.5$ (shown in solid lines of diminishing shades for diminishing ϵ) converge to the (a) Gibbs and (b) GGE results (shown with dashed lines). (c) Distances $d_{\ell=2}(\rho(t), \rho_\infty)$ for different initial temperatures $\beta \in [0, 0.2]$ and chaotic H at $\epsilon = 0.2$: no Mpemba effect is observed. (d) Crossing times t_{M_p} as a function of subsystem size ℓ for the integrable H extracted from $\rho_{\lambda}(t)$ calculated on $L = 400$. Parameters: $L = 80$ (chaotic TN results) and $L = 160$ (integrable TN results), with $160 \leq \chi \leq 240$.

[99]; see also the Supplementary Material. In the context of the Mpemba effect, Ref. [47] previously compared the behavior of the normalized Frobenius distance (5) with that of the trace distance. Our comparison for small system sizes, shown in End Matter, similarly supports the use of the normalized norm (5) over the bare Frobenius distance.

Results. We first test the extreme cases by considering the transverse field Ising Hamiltonian

$$H = \sum_j J \sigma_j^x \sigma_{j+1}^x + h_z \sigma_j^z + h_x \sigma_j^x, \quad (6)$$

for (a) chaotic parameters $J = 0.75$, $h_z = 1.0$, $h_x = 0.3$, when there are no additional conserved quantities besides the Hamiltonian itself ($N_C = 1$), and (b) integrable parameters $J = 0.75$, $h_z = 1.0$, $h_x = 0$, when the Hamiltonian commutes with macroscopically many conserved quantities ($N_C \sim 2L$). We use the dissipator (1) with $L_j = S_j^+ S_{j+1}^- + S_j^z + \frac{1}{2} \mathbb{1}_j$. However, our conclusions are not particular for this choice of Lindblad operators.

Fig. 2(a,b) shows distance $d_\ell(\rho(et), \rho_\infty)$, Eq. (5), as a function of the rescaled time et for the initial thermal states with a colder $\beta_c = 0.15$ (blue) and a hotter $\beta_h = 0$ (red) inverse temperature on support $\ell = 2$ for (a) chaotic H and (b) integrable H . According to our distance measure (5), the hotter initial state is farther away from the steady state. Solid lines denote different cou-

pling strengths, $\epsilon = 0.05, 0.2, 0.5$, with lighter shades corresponding to smaller ϵ , while dashed lines are extracted from the Gibbs and GGE approximation of the time evolution. In the rescaled time et , the finite coupling results indeed approach the (G)GE prediction $d_\ell(\rho_\lambda(et), \rho_{\lambda, \infty})$, with the distance (5) applied to the density matrices calculated from Eqs. (3,4), confirming that Gibbs and generalized Gibbs ensembles are the appropriate zeroth-order constituents of the expansion of weakly dissipative dynamics. Panels (a) and (b) suggest the absence of the Mpemba effect in the chaotic $N_C = 1$ case and its presence for the integrable $N_C \sim L$ case. In panel (c), we scan through different inverse temperatures $\beta \in [0, 0.2]$ of the initial state at $\epsilon = 0.2$ for the chaotic Hamiltonian, confirming the absence of a Mpemba effect when no additional conserved quantities are present. In panel (d), we show the dependence of the crossing time t_{M_p} in distances $d_\ell(\rho_\lambda(et), \rho_{\lambda, \infty})$ for the integrable H on support ℓ calculated with the GGE approximation on $L = 400$. We check that the results are converged with the full system size L . Although for our choice of parameters the crossing times remain $\mathcal{O}(1)$ at all ℓ , it is difficult to conclude whether they converge to a finite value for a thermodynamically large ℓ . This property can depend on the setup parameters and the choice of distance. We point out that experimentally relevant observables usually correspond to small ℓ , where we obtain a clear crossing.

From all cases considered, a consistent picture emerges: for the integrable, weakly open dynamics, the Mpemba effect is observed by measuring distances between the time-propagated state and the steady state, regardless of whether the system is coupled to the baths with an infinitesimal or finite strength. We discuss in the End Matter the interval of initial temperatures within which the Mpemba effect is observed. On the other hand, the Mpemba effect is generically not observed for the chaotic weakly open dynamics with a single approximately conserved quantity.

As underlined in the equation of motion (4), within the Gibbs ensemble approximation for chaotic Hamiltonians, the dissipative dynamics are constrained to a one-dimensional manifold of thermal states. If the dynamics starting from two different thermal states were to intersect at a Gibbs ensemble with the same temperature, both would then follow the same temperature trajectory, $\beta(t)$. This, however, does not occur: the evolution from different initial states is smooth and monotonic and the trajectories do not cross while relaxing toward the steady-state temperature (Fig. 2c). On the other hand, for an integrable Hamiltonian, Eq. (4) can be interpreted as an equation of motion in a multidimensional space of Lagrange parameters, spanning the manifold of all possible generalized Gibbs ensembles. Even when starting from a thermal one-dimensional sub-manifold, weakly dissipative evolution under the integrable Hamiltonian will generically take the dynamics into the higher-

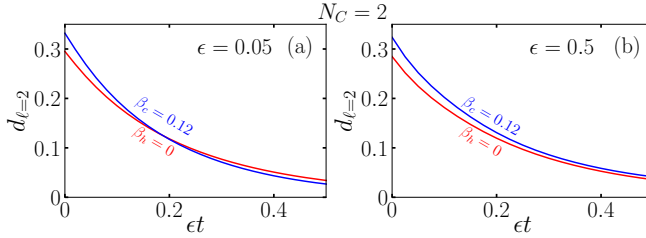


FIG. 3. Distances $d_{\ell}(\rho(t), \rho_{\infty})$ as a function of rescaled time et for the initial thermal states with $\beta_c = 0.12$ (blue) and $\beta_h = 0$ (red) inverse temperature and chemical potential $\mu(0) = 0$ for chaotic Hamiltonian with two conserved quantities, Eq. (7), at (a) $\epsilon = 0.05$ and (b) $\epsilon = 0.5$. Parameters: $L = 80$, $\ell = 2$, $\chi = 200$ (a), 160 (b).

dimensional GGE manifold, Fig. 1. Calculating the distance between the time-dependent GGE and the steady state projects the evolution from a multi-dimensional space to a single dimension, possibly allowing for crossing between trajectories corresponding to different initial states. The above arguments are based on equations of motion for the infinitesimally small coupling to baths. Importantly, our tensor network calculations at finite coupling ϵ support similar behavior also when the exact dynamics contains some small deviations from the thermal and generalized Gibbs ensembles.

While having one or macroscopically many conserved quantities are the extreme cases, one might ask whether having just two approximately conserved quantities is sufficient to observe the Mpemba effect in weakly dissipative dynamics. To examine this case, we consider

$$H = - \sum_j J(\sigma_j^x \sigma_{j+1}^x + \sigma_j^y \sigma_{j+1}^y) + \Delta_j \sigma_j^z \sigma_{j+1}^z \quad (7)$$

with $J = 1$, $\Delta_j = 1.2 + 0.4 \cdot (-1)^j$. The Hamiltonian (7) is not integrable, but has as an additional conserved quantity, the total magnetization $S^z = \sum_j \sigma_j^z$. As a dissipative perturbation, we consider Lindblad operators $L_i = \frac{1}{2} S_i^+ (\mathbb{1}_{i+1} - \sigma_{i+1}^z) + \sigma_i^x$, again coupled in the bulk. In this case, the steady state and the dissipative dynamics can be approximately described with a time dependent temperature and a chemical potential $\mu(t)$, associated with the approximately conserved magnetization. Importantly, we need a Lindblad perturbation that mixes magnetization sectors, otherwise we have a separate steady state in each sector and dynamics within a sector is as if we had a single approximately conserved quantity. Fig. 3(a) shows that the Mpemba effect is less pronounced, yet still visible, e.g., for initial temperatures $\beta_c = 0.12$, $\beta_h = 0$, chemical potential $\mu(0) = 0$ and the above choice for the dissipator. We note that a stronger dependence on the coupling strength to the baths is observed, with the Mpemba effect occurring only for sufficiently small $\epsilon \lesssim 0.2$; see Fig. 3(b) lacking the Mpemba effect at $\epsilon = 0.5$. Also, a finer tuning of the Lindblad op-

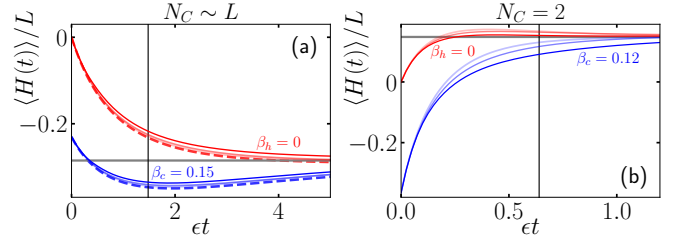


FIG. 4. Energy density $\langle H \rangle / L$ as a function of rescaled time et for (a) the integrable Hamiltonian (6) with $N_C \sim L$ and (b) the chaotic Hamiltonian with a single additional conserved quantity (7), $N_C = 2$. Parameters: $\epsilon = 0.05, 0.2, 0.5$, $L = 160$, $180 \leq \chi \leq 240$ ($N_C \sim L$) and $\epsilon = 0.05, 0.2, 0.5$, $L = 80$, $160 \leq \chi \leq 200$ ($N_C = 2$).

erators appears to be required for the effect to manifest.

Unlike previous examples, we see from Fig. 3 that the initial state of the hotter infinite temperature $\beta_h = 0$ is actually closer to the steady state than the colder $\beta_c = 0.12$. We are thus actually observing so called 'inverse Mpemba effect' [12, 17, 55]. However, for our model this is not such a surprise: while the Hamiltonian (7) has ferromagnetic interactions, the Lindblad operator prefers antiferromagnetic order, present in negative temperature states.

Discussion. Analysis on the level of distances is theoretically appropriate, but experimentally less feasible. In Fig. 4, we show how the quantum Mpemba effect manifests itself in terms of observables. We show energy density as a function of rescaled time et for (a) the integrable Hamiltonian (6) ($N_C \sim L$) and (b) the chaotic Hamiltonian (7) with an additional conserved quantity ($N_C = 2$). Again, solid lines denote finite coupling $\epsilon = 0.05, 0.2, 0.5$ results with diminishing shades for diminishing coupling strength and dashed lines the GGE result. The Mpemba effect does not manifest itself in a crossing. Rather, the energy density that was initially more distinct from the steady state value (denoted with the horizontal line for $\epsilon = 0.05$) gets at some finite time closer to it (for $\epsilon = 0.05$ denoted with the vertical line). In both cases the initially closer thermal state 'overshoots' the steady state energy density and approaches it nonmonotonically from the other direction. This behaviour has first been reported in Ref. [13], where the overshooting of the effective temperature was found to be consistent with the presence of the Mpemba effect.

The occurrence of the Mpemba effect in dissipative systems is often related to the orthogonality of the initial state to the slowest decaying mode [48–62]. An initial state that has zero overlap with the slowest decaying mode will decay at long times faster compared to states that have a finite overlap. The Mpemba effect can occur when such an initial state is at the same time farther away from the steady state than another non-orthogonal initial state. In the End Matter, we relate our main-text-

results on large system sizes to the exact diagonalization study of orthogonality to the slowest mode. The absence/presence of the Mpemba effect for a single/multiple conserved quantities corroborates with the orthogonality analysis for different initial thermal states.

Conclusions. In this paper, we discussed the occurrence of the Mpemba effect in weakly open quantum many-body systems, initialized in different thermal states. We give numerical evidence that the Mpemba effect can occur only when the underlying Hamiltonian has additional conserved quantities. Analytical arguments for our claim are based on the dimensional reduction. If energy is the only approximately conserved quantity, the dynamics can be approximated with evolution between Gibbs ensembles of different temperatures. In the presence of additional conserved quantities and for integrable Hamiltonians, additional time dependent Lagrange parameters must be introduced and the dynamics is approximated with time dependent generalized Gibbs ensembles. When projecting the dynamics on one-dimensional distances between the time-dependent state and the steady state, crossings can appear if the dynamics evolves on the multidimensional GGE manifold and cannot appear for dynamics within one-dimensional thermal manifold. Even though our dimensional-reduction argument applies at the level of the zeroth-order approximation, tensor-network simulations of the full density matrix suggest our claim is valid for finite, experimentally relevant bath couplings. Furthermore, our conclusions are system-size independent and capture genuine many-body phenomena.

In future work, it would be valuable to test the implications of our arguments in other, even more common setups. For instance, one could examine whether (approximate) integrability can realize sufficiently nonthermal transient dynamics even when the baths are thermal. The Mpemba effect could occur when conserved quantities are additionally perturbed with unitary sources, such as weak integrability-breaking terms in the Hamiltonian, and coupling such systems to thermal baths is of particular relevance for possible realizations with nearly integrable spin-chain materials. As we observed that a finer tuning of Lindblad operators is needed to observe the Mpemba effect in chaotic systems with only a single additional conserved quantity, it remains to be understood how generic this effect is or what baths are required to observe it. Another promising direction is to relate our arguments to the occurrence of the Mpemba effect in classical systems, in connection with their symmetries. Finally, our general conclusions may facilitate experimental verification using quantum simulators, quantum computers, or strongly correlated materials.

We thank S. Murciano, P. Calabrese and G. Teza for useful discussions. I.U, G.L. and Z.L acknowledge the support by P1-0044 program of the Slovenian Research Agency, the QuantERA grant QuSiED by MVZI, Quan-

tERA II JTC 2021, and ERC StG 2022 project DrumS, Grant Agreement 101077265. R.S. acknowledges support from ERC Advanced grant No. 101096208– QUEST, and Research Programme P1-0402 of Slovenian Research and Innovation Agency (ARIS). Calculations were performed at the cluster ‘spinon’ of JSI, Ljubljana, using QuSpin [100] and ITensors.jl [101].

- [1] E. B. Mpemba and D. G. Osborne, Cool?, *Phys. Educ.* **4**, 172 (1969).
- [2] A. Greaney, G. Lani, G. Cicero, and J. C. Grossman, Mpemba-like behavior in carbon nanotube resonators, *Metall. Mater. Trans. A* **42**, 3907 (2011).
- [3] Y. H. Ahn, H. Kang, D. Y. Koh, and H. Lee, Experimental verifications of mpemba-like behaviors of clathrate hydrates, *Korean J. Chem. Eng.* **33**, 1903 (2016).
- [4] A. Lasanta, F. V. Reyes, A. Prados, and A. Santos, When the hotter cools more quickly: Mpemba effect in granular fluids, *Phys. Rev. Lett.* **119**, 148001 (2017).
- [5] T. Keller, V. Torggler, S. B. Jäger, S. Schutz, H. Ritsch, and G. Morigi, Quenches across the self-organization transition in multimode cavities, *New J. Phys.* **20**, 025004 (2018).
- [6] C. Hu, J. Li, S. Huang, H. Li, C. Luo, J. Chen, S. Jiang, and L. An, Conformation directed mpemba effect on polylactide crystallization, *Cryst. Growth Des.* **18**, 5757 (2018).
- [7] M. Baity-Jesi, E. Calore, A. Cruz, L. A. Fernandez, J. M. Gil-Narvío, A. Gordillo-Guerrero, D. Iñiguez, A. Lasanta, A. Maiorano, E. Marinari, V. Martín-Mayor, J. Moreno-Gordo, A. Muñoz-Sudupe, D. Navarro, G. Parisi, S. Perez-Gaviro, F. Ricci-Tersenghi, J. J. Ruiz-Lorenzo, S. F. Schifano, B. Seoane, A. Tarancón, R. Tripiccione, and D. Yllanes, The mpemba effect in spin glasses is a persistent memory effect, *PNAS* **116**, 15350 (2019).
- [8] F. J. Schwarzenbach and H. Löwen, Anomalous cooling and overcooling of active colloids, *Phys. Rev. Lett.* **129**, 138002 (2022).
- [9] R. Holtzman and O. Raz, Landau theory for the mpemba effect through phase transitions, *Commun. Phys.* **5**, 280 (2022).
- [10] G. Teza, R. Yaacoby, and O. Raz, Relaxation shortcuts through boundary coupling, *Phys. Rev. Lett.* **131**, 017101 (2023).
- [11] I. G.-A. Pemartín, E. Mompó, A. Lasanta, V. Martín-Mayor, and J. Salas, Shortcuts of freely relaxing systems using equilibrium physical observables, *Phys. Rev. Lett.* **132**, 117102 (2024).
- [12] Z. Lu and O. Raz, Nonequilibrium thermodynamics of the markovian mpemba effect and its inverse, *PNAS* **114**, 5083 (2017).
- [13] I. Klich, O. Raz, O. Hirschberg, and M. Vučelja, Mpemba index and anomalous relaxation, *Phys. Rev. X* **9**, 021060 (2019).
- [14] A. Kumar and J. Bechhoefer, Exponentially faster cooling in a colloidal system, *Nature* **584**, 64 (2020).
- [15] J. Bechhoefer, A. Kumar, and R. Chétrite, A fresh understanding of the mpemba effect, *Nat Rev Phys.* **3**, 534

(2021).

[16] A. Gal and O. Raz, Precooling strategy allows exponentially faster heating, *Phys. Rev. Lett.* **124**, 060602 (2020).

[17] A. Kumar, R. Chétrite, and J. Bechhoefer, Anomalous heating in a colloidal system, *PNAS* **119**, e2118484119 (2022).

[18] M. R. Walker and M. Vucelja, Mpemba effect in terms of mean first passage times of overdamped langevin dynamics on a double-well potential, [arXiv:2212.07496](https://arxiv.org/abs/2212.07496) (2022).

[19] M. R. Walker, S. Bera, and M. Vucelja, Optimal transport and anomalous thermal relaxations, [arXiv:2307.16103](https://arxiv.org/abs/2307.16103) (2023).

[20] S. Bera, M. R. Walker, and M. Vucelja, Effect of dynamics on anomalous thermal relaxations and information exchange, [arXiv:2308.04557](https://arxiv.org/abs/2308.04557) (2023).

[21] A. Santos, Mpemba meets newton: Exploring the mpemba and kovacs effects in the time-delayed cooling law, *Phys. Rev. E* **109**, 044149 (2024).

[22] T. Van Vu and H. Hayakawa, Thermomajorization mpemba effect, *Phys. Rev. Lett.* **134**, 107101 (2025).

[23] G. Teza, J. Bechhoefer, A. Lasanta, O. Raz, and M. Vucelja, Speedups in nonequilibrium thermal relaxation: Mpemba and related effects, [arXiv:2502.01758](https://arxiv.org/abs/2502.01758) (2025).

[24] H. C. Burridge and P. F. Linden, Questioning the mpemba effect: Hot water does not cool more quickly than cold, *Sci Rep* **6**, 37665 (2016).

[25] H. C. Burridge and O. Hallstadius, Observing the mpemba effect with minimal bias and the value of the mpemba effect to scientific outreach and engagement, *Proc. R. Soc. A.* **476**, 20190829 (2020).

[26] F. Ares, P. Calabrese, and S. Murciano, The quantum mpemba effects, *Nat Rev Phys* **7**, 451 (2025).

[27] F. Ares, S. Murciano, and P. Calabrese, Entanglement asymmetry as a probe of symmetry breaking, *Nat Commun* **14**, 2036 (2023).

[28] F. Ares, S. Murciano, E. Vernier, and P. Calabrese, Lack of symmetry restoration after a quantum quench: an entanglement asymmetry study, *SciPost Phys.* **15**, 089 (2023).

[29] S. Murciano, F. Ares, I. Klich, and P. Calabrese, Entanglement asymmetry and quantum mpemba effect in the xy spin chain, *J. Stat. Mech.* **2024**, 013103 (2024).

[30] C. Rylands, E. Vernier, and P. Calabrese, Dynamical symmetry restoration in the heisenberg spin chain, *J. Stat. Mech.* **2024**, 123102 (2024).

[31] L. K. Joshi, J. Franke, A. Rath, F. Ares, S. Murciano, F. Kranzl, R. Blatt, P. Zoller, B. Vermersch, P. Calabrese, C. F. Roos, and M. K. Joshi, Observing the quantum mpemba effect in quantum simulations, *Phys. Rev. Lett.* **133**, 010402 (2024).

[32] P. Calabrese and J. Cardy, Evolution of entanglement entropy in one-dimensional systems, *J. Stat. Mech.* **2005**, P04010 (2005).

[33] V. Alba and P. Calabrese, Entanglement and thermodynamics after a quantum quench in integrable systems, *Proc. Natl. Acad. Sci. U.S.A.* **114**, 7947 (2017).

[34] V. Alba and P. Calabrese, Entanglement dynamics after quantum quenches in generic integrable systems, *SciPost Phys.* **4**, 017 (2018).

[35] C. Rylands, K. Klobas, F. Ares, P. Calabrese, S. Murciano, and B. Bertini, Microscopic origin of the quantum mpemba effect in integrable systems, *Phys. Rev. Lett.* **133**, 010401 (2024).

[36] K. Klobas, Non-equilibrium dynamics of symmetry-resolved entanglement and entanglement asymmetry: exact asymptotics in rule 54*, *J. Phys. A: Math. Theor.* **57**, 505001 (2024).

[37] X. Turkeshi, P. Calabrese, and A. D. Luca, Quantum mpemba effect in random circuits, [arXiv:2405.14514](https://arxiv.org/abs/2405.14514) (2024).

[38] S. Liu, H.-K. Zhang, S. Yin, and S.-X. Zhang, Symmetry restoration and quantum mpemba effect in symmetric random circuits, *Phys. Rev. Lett.* **133**, 140405 (2024).

[39] K. Klobas, C. Rylands, and B. Bertini, Translation symmetry restoration under random unitary dynamics, *Phys. Rev. B* **111** (2025).

[40] H. Yu, Z.-X. Li, and S.-X. Zhang, Symmetry breaking dynamics in quantum many-body systems, *Chin. Phys. Lett.* (2025).

[41] F. Ares, S. Murciano, P. Calabrese, and L. Piroli, Entanglement asymmetry dynamics in random quantum circuits, *Phys. Rev. Research* **7** (2025).

[42] A. Foligno, P. Calabrese, and B. Bertini, Nonequilibrium dynamics of charged dual-unitary circuits, *PRX Quantum* **6**, 010324 (2025).

[43] S. Aditya, A. Summer, P. Sierant, and X. Turkeshi, Mpemba effects in quantum complexity, [arXiv:2509.22176](https://arxiv.org/abs/2509.22176) (2025).

[44] S. Liu, H.-K. Zhang, S. Yin, S.-X. Zhang, and H. Yao, Symmetry restoration and quantum mpemba effect in many-body localization systems, *Science Bulletin* <https://doi.org/10.1016/j.scib.2025.10.017> (2025).

[45] S. Yamashika, F. Ares, and P. Calabrese, Entanglement asymmetry and quantum mpemba effect in two-dimensional free-fermion systems, *Phys. Rev. B* **110**, 085126 (2024).

[46] S. Yamashika, P. Calabrese, and F. Ares, Quenching from superfluid to free bosons in two dimensions: Entanglement, symmetries, and the quantum mpemba effect, *Phys. Rev. A* **111**, 043304 (2025).

[47] T. Bhore, L. Su, I. Martin, A. A. Clerk, and Z. Papić, Quantum mpemba effect without global symmetries, *Phys. Rev. B* **112**, L121109 (2025).

[48] F. Carollo, A. Lasanta, and I. Lesanovsky, Exponentially accelerated approach to stationarity in markovian open quantum systems through the mpemba effect, *Phys. Rev. Lett.* **127**, 060401 (2021).

[49] M. Moroder, O. Culhane, K. Zawadzki, and J. Goold, Thermodynamics of the quantum mpemba effect, *Phys. Rev. Lett.* **133**, 140404 (2024).

[50] S. Kochsiek, F. Carollo, and I. Lesanovsky, Accelerating the approach of dissipative quantum spin systems towards stationarity through global spin rotations, *Phys. Rev. A* **106**, 012207 (2022).

[51] R. Bao and Z. Hou, Accelerating quantum relaxation via temporary reset: A mpemba-inspired approach, *Phys. Rev. Lett.* **135**, 150403 (2025).

[52] L. P. Bettmann and J. Goold, Information geometry approach to quantum stochastic thermodynamics, *Phys. Rev. E* **111**, 014133 (2025).

[53] A. K. Chatterjee, S. Takada, and H. Hayakawa, Quantum mpemba effect in a quantum dot with reservoirs, *Phys. Rev. Lett.* **131**, 080402 (2023).

[54] A. K. Chatterjee, S. Takada, and H. Hayakawa, Multiple quantum mpemba effect: exceptional points and

oscillations, *Phys. Rev. A* **110**, 022213 (2024).

[55] S. A. Shapira, Y. Shapira, J. Markov, G. Teza, N. Akerman, O. Raz, and R. Ozeri, Inverse mpemba effect demonstrated on a single trapped ion qubit, *Phys. Rev. Lett.* **133**, 010403 (2024).

[56] F. Ivander, N. Anto-Sztrikacs, and D. Segal, Hyperacceleration of quantum thermalization dynamics by bypassing long-lived coherences: An analytical treatment, *Phys. Rev. E* **108**, 014130 (2023).

[57] Y.-L. Zhou, X.-D. Yu, C.-W. Wu, X.-Q. Li, J. Zhang, W. Li, and P. Chen, Accelerating relaxation through liouvillian exceptional point, *Phys. Rev. Research* **5**, 043036 (2023).

[58] D. Liu, J. Yuan, H. Ruan, Y. Xu, S. Luo, J. He, X. He, Y. Ma, and J. Wang, Speeding up quantum heat engines by the mpemba effect, *Phys. Rev. A* **110**, 042218 (2024).

[59] J. Furtado and A. C. Santos, Enhanced quantum mpemba effect with squeezed thermal reservoirs, *Ann. Phys.* **480**, 170135 (2025).

[60] I. Medina, O. Culhane, F. C. Binder, G. T. Landi, and J. Goold, Anomalous discharging of quantum batteries: The ergotropic mpemba effect, *Phys. Rev. Lett.* **134**, 220402 (2025).

[61] J. Graf, J. Splettstoesser, and J. Monsel, Role of electron-electron interaction in the mpemba effect in quantum dots, *J. Phys.: Condens. Matter* **37**, 195302 (2025).

[62] P. Westhoff, S. Paeckel, and M. Moroder, Fast and direct preparation of a genuine lattice bec via the quantum mpemba effect, *arXiv:2504.05549* (2025).

[63] X. Wang and J. Wang, Mpemba effects in nonequilibrium open quantum systems, *Phys. Rev. Research* **6**, 033330 (2024).

[64] D. Qian, H. Wang, and J. Wang, Intrinsic quantum mpemba effect in markovian systems and quantum circuits, *Phys. Rev. B* **111**, L220304 (2025).

[65] M. Boubakour, S. Endo, T. Fogarty, and T. Busch, Dynamical invariant based shortcut to equilibration in open quantum systems, *Quantum Sci. Technol.* **10**, 025036 (2025).

[66] S. Longhi, Mpemba effect and super-accelerated thermalization in the damped quantum harmonic oscillator, *Quantum* **9**, 1677 (2025).

[67] F. Kheirandish, N. Cheraghpour, and A. Moradian, The mpemba effect in quantum oscillating and two-level systems, *Physics Letters A* **559**, 130915 (2025).

[68] A. Nava and R. Egger, Mpemba effects in open nonequilibrium quantum systems, *Phys. Rev. Lett.* **133**, 136302 (2024).

[69] J. Zhang, G. Xia, C.-W. Wu, T. Chen, Q. Zhang, Y. Xie, W.-B. Su, W. Wu, C.-W. Qiu, P. Chen, W. Li, H. Jing, and Y.-L. Zhou, Observation of quantum strong mpemba effect, *Nat Commun* **16**, 301 (2025).

[70] M. E. Edo and L.-A. Wu, Study on quantum thermalization from thermal initial states in a superconducting quantum computer, *arXiv:2403.14630* (2024).

[71] A. Nava and M. Fabrizio, Lindblad dissipative dynamics in the presence of phase coexistence, *Phys. Rev. B* **100**, 125102 (2019).

[72] X. Wang, J. Su, and J. Wang, Mpemba meets quantum chaos: Anomalous relaxation and mpemba crossings in dissipative sachdev-ye-kitaev models, *arXiv:2410.06669* (2024).

[73] S. Longhi, Photonic mpemba effect, *Opt. Lett.* **49**, 5188 (2024).

[74] S. Longhi, Bosonic mpemba effect with non-classical states of light, *APL Quantum* **1**, 046110 (2024).

[75] D. Auerbach, Supercooling and the mpemba effect: When hot water freezes quicker than cold, *Am. J. Phys.* **63**, 882 (1995).

[76] S. Esposito, R. D. Risi, and L. Somma, Mpemba effect and phase transitions in the adiabatic cooling of water before freezing, *Physica A* **387**, 757 (2008).

[77] F. Ares, V. Vitale, and S. Murciano, Quantum mpemba effect in free-fermionic mixed states, *Phys. Rev. B* **111**, 104312 (2025).

[78] Z. Lenarčič, F. Lange, and A. Rosch, Perturbative approach to weakly driven many-particle systems in the presence of approximate conservation laws, *Phys. Rev. B* **97**, 024302 (2018).

[79] Z. Lenarčič, E. Altman, and A. Rosch, Activating many-body localization in solids by driving with light, *Phys. Rev. Lett.* **121**, 267603 (2018).

[80] Z. Lenarčič, O. Alberton, A. Rosch, and E. Altman, Critical behavior near the many-body localization transition in driven open systems, *Phys. Rev. Lett.* **125**, 116601 (2020).

[81] T. Shirai and T. Mori, Thermalization in open many-body systems based on eigenstate thermalization hypothesis, *Phys. Rev. E* **101**, 042116 (2020).

[82] F. Lange, Z. Lenarčič, and A. Rosch, Pumping approximately integrable systems, *Nat. Commun.* **8**, 1 (2017).

[83] F. Lange, Z. Lenarčič, and A. Rosch, Time-dependent generalized Gibbs ensembles in open quantum systems, *Phys. Rev. B* **97**, 165138 (2018).

[84] F. Reiter, F. Lange, S. Jain, M. Grau, J. P. Home, and Z. Lenarčič, Engineering generalized Gibbs ensembles with trapped ions, *Phys. Rev. Res.* **3**, 033142 (2021).

[85] M. Schmitt and Z. Lenarčič, From observations to complexity of quantum states via unsupervised learning, *Phys. Rev. B* **106**, L041110 (2022).

[86] I. Ulčakar and Z. Lenarčič, Iterative construction of conserved quantities in dissipative nearly integrable systems, *Phys. Rev. Lett.* **132**, 230402 (2024).

[87] I. Ulčakar and Z. Lenarčič, Generalized Gibbs ensembles in weakly interacting dissipative systems and digital quantum computers, *arXiv:2406.17033* (2024).

[88] I. Bouchoule, B. Doyon, and J. Dubail, The effect of atom losses on the distribution of rapidities in the one-dimensional Bose gas, *SciPost Phys.* **9**, 044 (2020).

[89] D. Rossini, A. Ghermaoui, M. B. Aguilera, R. Vatré, R. Bouganne, J. Beugnon, F. Gerbier, and L. Mazza, Strong correlations in lossy one-dimensional quantum gases: From the quantum Zeno effect to the generalized Gibbs ensemble, *Phys. Rev. A* **103**, L060201 (2021).

[90] F. Gerbino, I. Lesanovsky, and G. Perfetto, Large-scale universality in quantum reaction-diffusion from keldysh field theory, *Phys. Rev. B* **109**, L220304 (2024).

[91] G. Perfetto, F. Carollo, J. P. Garrahan, and I. Lesanovsky, Reaction-Limited Quantum Reaction-Diffusion Dynamics, *Phys. Rev. Lett.* **130**, 210402 (2023).

[92] S. Rowlands, I. Lesanovsky, and G. Perfetto, Quantum reaction-limited reaction-diffusion dynamics of noninteracting bose gases, *New J. Phys.* **26**, 043010 (2024).

[93] F. Riggio, L. Rosso, D. Karevski, and J. Dubail, Effects of atom losses on a one-dimensional lattice gas of hardcore bosons, *Phys. Rev. A* **109**, 023311 (2024).

[94] E. Starchl and L. M. Sieberer, Relaxation to a parity-

time symmetric generalized gibbs ensemble after a quantum quench in a driven-dissipative kitaev chain, *Phys. Rev. Lett.* **129**, 220602 (2022).

[95] E. Starchl and L. M. Sieberer, Quantum quenches in driven-dissipative quadratic fermionic systems with parity-time symmetry, *Phys. Rev. Res.* **6**, 013016 (2024).

[96] L. Lumia, G. Aupetit-Diallo, J. Dubail, and M. Collura, Accuracy of a time-dependent generalized gibbs ensemble approach under weak dissipation, *Phys. Rev. A* **112**, 012206 (2025).

[97] M. Zwolak and G. Vidal, Mixed-state dynamics in one-dimensional quantum lattice systems: A time-dependent superoperator renormalization algorithm, *Phys. Rev. Lett.* **93**, 207205 (2004).

[98] U. Schollwöck, The density-matrix renormalization group in the age of matrix product states, *Ann. Phys.* **326**, 96 (2011), january 2011 Special Issue.

[99] M. Fagotti and F. H. L. Essler, Reduced density matrix after a quantum quench, *Phys. Rev. B* **87**, 245107 (2013).

[100] P. Weinberg and M. Bukov, Quspin: a python package for dynamics and exact diagonalization of quantum many-body systems. part i: The spin chain problem, *Computer Physics Communications* **282**, 106 (2023).

[101] M. Fishman, S. R. White, and E. M. Stoudenmire, The ITensor Software Library for Tensor Network Calculations, *SciPost Phys. Codebases* **4** (2022).

[102] M. Fagotti and P. Calabrese, Entanglement entropy of two disjoint blocks in xy chains, *J. Stat. Mech.* **2010**, P04016 (2010).

END MATTER

The Quantum Mpemba effect in dissipative systems is in most cases related with the orthogonality to the slowest decaying mode of the Liouvillian [48–62]. Namely, initializing the system in a state that is orthogonal to the slowest decaying mode should result in a faster relaxation to the steady state compared to an initial state with a finite overlap with the slowest mode, which is initially closer to the steady state.

The explicit construction of the orthogonalisation procedure by diagonalizing the Liouvillian is practically difficult and limits the accessible system sizes. In the main text, we showed that the density matrix dynamics can be approximated with (G)GEs. However, without any further assumptions, following bare perturbative arguments for weak dissipation [78], the slow dynamics happens within the diagonal subspace, spanned by exponentially many projectors on the Hamiltonian eigenstates $|m\rangle\langle m|$. I.e., the slowest mode primarily lies in this manifold and also the initial thermal states are fully embedded in the diagonal subspace. The slow dynamics is captured by the Liouvillian projected onto this subspace of matrices. To perform the orthogonality analysis we thus resort to the diagonalization of the projected Liouvillian, represented by the matrix $D_{mn} = \langle m|(\hat{D}|n\rangle\langle n|)|m\rangle$. This al-

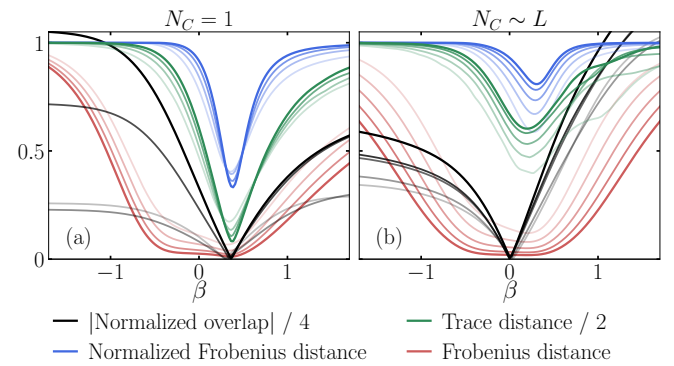


FIG. 5. Normalized overlap of different thermal states with the slowest mode and different distances (trace distance, Frobenius distance, normalized Frobenius distance) of thermal states to the steady state for (a) chaotic and (b) integrable transverse field Ising parameters used in the main text. System sizes (a) $L = 8, 10, 12, 14$ and (b) $L = 10, 12, 14, 16$ from lighter to darker colors.

lows us to study somewhat larger system sizes $L \leq 16$, compared to the analysis that would be performed on the non-projected Liouvillian.

Fig. 5 shows normalized overlaps of different initial thermal states ρ_β , characterized by the inverse temperature β , and the left eigenvector $\rho_{\text{slow}}^{(l)}$, corresponding to the slowest right eigenvector $\rho_{\text{slow}}^{(r)}$ of the projected Liouvillian, $\|\rho_{\text{slow}}^{(r)}\|_1 * \text{Tr}[(\rho_{\text{slow}}^{(l)})^\dagger \rho_\beta]$. Normalization is chosen to avoid any ambiguity regarding the separate normalization of the left and right eigenvectors, under the standard assumption $\text{Tr}[(\rho_i^{(l)})^\dagger \rho_j^{(r)}] = \delta_{ij}$. Fig. 5(a) shows result for the chaotic choice of transverse field Ising parameters, while panel (b) shows results for the integrable parameters. For both cases, there exists a thermal initial state that is orthogonal to the slowest mode. Different shades correspond to different system sizes, from lighter to darker shade for increasing system sizes $L = 8, 10, 12, 14, 16$. Whether this can allow for the occurrence of the Mpemba effect depends on the distance of the initial thermal state to the steady state, on Fig. 5 shown for different definitions of distance: the trace distance $d_T(\rho_\beta, \rho_\infty^{(D)}) = \text{Tr}[\sqrt{(\rho_\beta - \rho_\infty^{(D)})^2}]$, the Frobenius distance $d_F(\rho_\beta, \rho_\infty^{(D)}) = \sqrt{\text{Tr}[(\rho_\beta - \rho_\infty^{(D)})^2]}$ and the normalized Frobenius distance $d_L(\rho_\beta, \rho_\infty^{(D)}) = \sqrt{\text{Tr}[(\rho_\beta - \rho_\infty^{(D)})^2]/(\text{Tr}[(\rho_\beta)^2] + \text{Tr}[(\rho_\infty^{(D)})^2])}$. Here we considered the steady state projected to the diagonal subspace, $\rho_\infty^{(D)}$. Again, increasingly darker shades correspond to the same increasingly larger system sizes. The most important conclusion from the above analysis is that for the chaotic model with a single conserved quantity, the initial thermal state that is orthogonal to the slowest mode is also the state that is closest to the steady state, ruling out the observation of the Mpemba

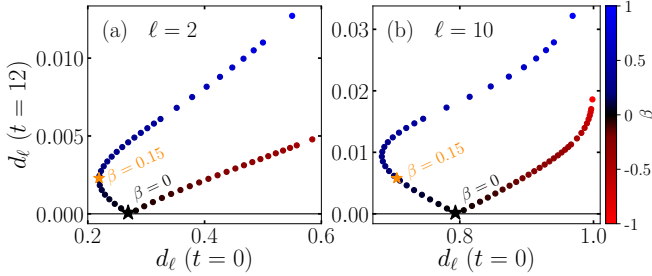


FIG. 6. Integrable transverse field Ising model: Initial distance $[d_\ell(\rho_\lambda(0), \rho_\infty)]$ on the x-axis and finite time $\ell t = 12$ distance $d_\ell(\rho_\lambda(\ell t), \rho_\infty)$ on the y-axis for different inverse temperatures $\beta \in [-1, 1]$. Pairs of initial temperatures that are connected with a line of negative slope have by time $\ell t = 12$ gone through the crossing point. Results are shown for subsystem size (a) $\ell = 2$ and (b) $\ell = 10$.

effect. With increasing system sizes minima in different distances are just deepening, since in the thermodynamic limit the diagonal projection of the steady state is also a thermal state and thus orthogonal to the other decaying modes. On the other hand, for the integrable model in panel (b), the dip in the distances is at a different temperature and is getting shallower with increasing system sizes where the GGE character of the steady state is becoming more pronounced. In the interval of initial state temperatures between the minima of the overlap with the slowest mode and the distance to the steady state are pairs of initial temperatures for which the Mpemba effect could be observed. A secondary observation is that various distances behave qualitatively similar but quantitatively different. Trace and normalized Frobenius distance are somewhat more similar, which is the reason why we used the latter also in the main text. Previously it was already pointed out by Ref. [99] that the normalized Frobenius distance captures the comparison of observables and reduced density matrices in the two states considered better than the bare Frobenius distance.

Conclusions from Fig. 5(b) for the integrable transverse field Ising model are confirmed also in Fig. 6, where by scanning through different initial temperatures, we plot on the x-axis the initial normalized Frobenius distance to the steady state $d_\ell(\rho_\lambda(0), \rho_\lambda(t \rightarrow \infty))$ and on the y-axis the distance at a later time $d_\ell(\rho_\lambda(\ell t = 12), \rho_\lambda(t \rightarrow \infty))$. On panel (a) we show results for the distance on subsystem size $\ell = 2$ and on (b) for $\ell = 10$. Pairs of temperatures that are connected with a line of negative slope have by time $\ell t = 12$ gone through the crossing point. As we can see from this plot, any pairs of temperature from the interval $[\beta_h, \beta_c] = [0, 0.15]$ will do that though the interval depends on the subsystems size.

Next, we perform a similar analysis for the chaotic model (7) with Lindblad operators $L_i = \frac{1}{2}S_i^+(\mathbb{1}_{i+1} - \sigma_{i+1}^z) + \sigma_i^x$, shown in the main text as an example of a setup with two approximately conserved quantities.

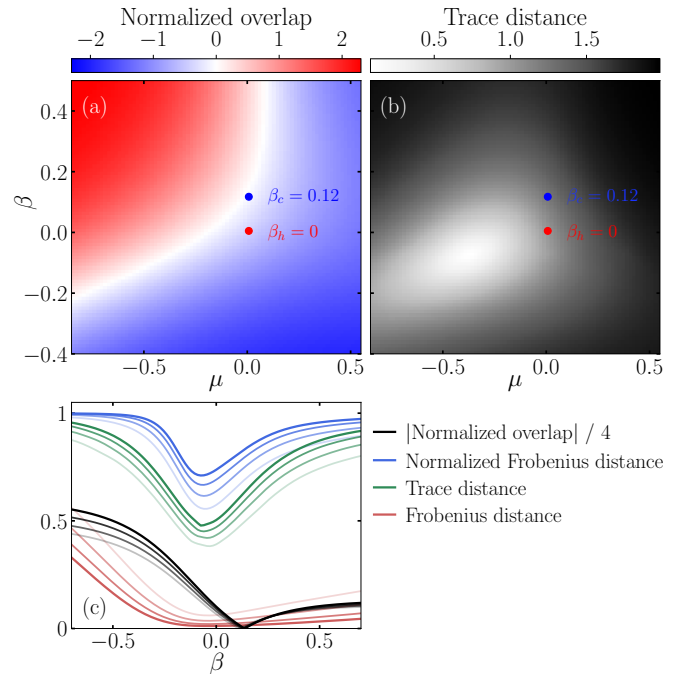


FIG. 7. Orthogonality analysis for model (7). (a) Normalized overlap of states parametrized with inverse temperature β and chemical potential μ with the slowest mode. (b) Trace distance between the steady state and the initial states parametrized with inverse temperature β and chemical potential μ . System size $L = 14$. (c) Normalized overlap with the slowest mode and different distances (trace distance, normalized Frobenius distance and Frobenius distance) of initial thermal states ($\mu = 0$) to the steady state, $L = 8, 10, 12, 14$ from lighter to darker colors.

Here, we perform the same analysis as in Fig. 5, but for the initial states $\rho_{\beta, \mu}$ characterized with inverse temperature β and chemical potential μ , associated with total S^z . Panel (a) shows contour plots for the normalized overlap $\|\rho_{\text{slow}}^{(r)}\|_1 * \text{Tr}[(\rho_{\text{slow}}^{(l)})^\dagger \rho_{\beta, \mu}]$ with the slowest mode, while panel (b) shows trace distance of such initial states to the diagonal projection of the steady state $d_T(\rho_{\beta, \mu}, \rho_\infty^{(D)})$ for $L = 8, 10, 12, 14$. Again, there are pairs of parameters (β, μ) for which the initial state is (nearly) orthogonal to the slowest mode and yet further away from the steady state. Pairs of initial states shown in the main text in Fig. 3 are denoted with dots of the corresponding color. Panel (c) focuses on the initial states with $\mu = 0$ and shows the normalized overlap of initial $\rho_{\beta, \mu=0}$ with the slowest mode, the trace $d_T(\rho_{\beta, \mu=0}, \rho_\infty^{(D)})$, the Frobenius distance $d_F(\rho_{\beta, \mu=0}, \rho_\infty^{(D)})$ and the normalized Frobenius distance $d_L(\rho_{\beta, \mu=0}, \rho_\infty^{(D)})$ as a function of β . Orthogonality condition around $\beta = 0.12$ motivates our choice presented in the main text, $\beta_c = 0.12$ and $\beta_h = 0$.

Supplemental Material: Conserved quantities enable the quantum Mpemba effect in weakly open systems

Iris Ulčakar^{1,2}, Gianluca Lagnese¹, Rustem Sharipov², and Zala Lenarčič¹

¹*Department of Theoretical Physics, J. Stefan Institute, SI-1000 Ljubljana, Slovenia*

²*Faculty for Mathematics and Physics, University of Ljubljana, Jadranska ulica 19, 1000 Ljubljana, Slovenia*

In the Supplemental Material, we (i) summarize the calculation of dynamics within the generalized Gibbs ensemble approximation in the free fermion language, and (ii) explain how to evaluate distances between such Gaussian states.

Free fermion representation of the transverse field Ising Hamiltonian

Here, we discuss how to efficiently reformulate the problem for the integrable transverse field Ising model

$$H = \sum_i J \sigma_i^x \sigma_{i+1}^x + h_z \sigma_i^z, \quad (\text{S2})$$

in terms of fermionic operators, so as to evaluate the equation of motion (3) in thermodynamically large systems using Wick contractions for Gaussian states. Same treatment has already been performed in Ref. [87], we repeat it here for completeness.

Non-interacting Hamiltonian (S2) can be diagonalized using a sequence of transformations: the Jordan-Wigner transformation $\sigma_j^z = 2c_j^\dagger c_j - 1$, $\sigma_j^+ = e^{i\pi \sum_{l < j} n_l} c_j^\dagger$, the Fourier transform $c_j = \frac{e^{-i\pi/4}}{\sqrt{L}} \sum_q e^{iqj} c_q$, and the Bogoliubov transformation $c_q = u_q d_q - v_q d_{-q}^\dagger$ with $u_q = 2(J \cos q + h_z)$, $b_q = -2J \sin q$, $u_q = \frac{\varepsilon_q + a_q}{\sqrt{2\varepsilon_q(\varepsilon_q + a_q)}}$, $v_q = \frac{b_q}{\sqrt{2\varepsilon_q(\varepsilon_q + a_q)}}$. Finally, the Hamiltonian is written in terms of quasiparticle occupation operators $n_q = d_q^\dagger d_q$ and dispersion $\varepsilon_q = 2\sqrt{J^2 + 2h_z J \cos q + h_z^2}$, as

$$H = \sum_q \varepsilon_q \left(n_q - \frac{1}{2} \right). \quad (\text{S3})$$

In the fermionic language, the zeroth order generalized Gibbs ensemble approximation to the dynamic can be parametrized with chemical potentials $\mu_q(t)$, associated with occupation operators n_q ,

$$\rho_\lambda(t) = \frac{e^{-\sum_q \mu_q(t) n_q}}{\text{Tr}[e^{-\sum_q \mu_q(t) n_q}].} \quad (\text{S4})$$

For these calculations, we use periodic boundary conditions in the spin formulation, which are translated to periodic boundary conditions in the fermion picture for an odd number of particles and anti-periodic for an even number of particles. The two parity sectors contain different wave vectors $\mathcal{K}^+ = \{\frac{2\pi}{L}(q + \frac{1}{2}), q = 0, \dots, L-1\}$ (even sector) and $\mathcal{K}^- = \{\frac{2\pi}{L}q, q = 0, \dots, L-1\}$ (odd sector).

In order to evaluate the equation of motion (Eq. (3) from the main text) for the occupation operator,

$$\langle \dot{n}_q \rangle = \epsilon \sum_j \text{Tr}[L_j^\dagger n_q L_j \rho(t)] - \text{Tr}[n_q L_j^\dagger L_j \rho(t)] \quad (\text{S5})$$

we need to express the Lindblad operators considered $L_j = S_j^+ S_{j+1}^- + S_j^z + \frac{1}{2} \mathbb{1}_j$ in terms of Bogoliubov modes

$$L_j = \sum_{q,q'} \frac{e^{-ij(q-q')}}{L} (1 + e^{iq'}) (u_q d_q^\dagger - v_q d_{-q}) (u_{q'} d_{q'}^\dagger - v_{q'} d_{-q'}^\dagger). \quad (\text{S6})$$

Using Wick contractions, Eq. (S5) can be simplified into a compact scattering equation

$$\begin{aligned} \langle \dot{n}_q \rangle = & \frac{2\epsilon}{L} \sum_{q'} f_{q,q'}^s (1 - n_q) \langle n_{q'} \rangle - f_{q',q}^s \langle n_q \rangle \langle 1 - n_{q'} \rangle \\ & + f_{q,q'}^c \langle 1 - n_q \rangle \langle 1 - n_{q'} \rangle - f_{q,q'}^a \langle n_q \rangle \langle n_{q'} \rangle. \end{aligned} \quad (\text{S7})$$

parametrized with positive functions encoding the scattering processes

$$\begin{aligned} f_{q,q'}^s = & u_q^2 u_{q'}^2 (1 + \cos q') + v_q^2 v_{q'}^2 (1 + \cos q) \\ & - u_q v_q u_{q'} v_{q'} (1 + \cos q' + \cos q + \cos(q + q')), \end{aligned} \quad (\text{S8})$$

the creation of q' and q modes

$$\begin{aligned} f_{q',q}^c = & v_q^2 u_{q'}^2 (1 + \cos q) + u_q^2 v_{q'}^2 (1 + \cos q') \\ & - u_q v_q u_{q'} v_{q'} (1 + \cos q' + \cos q + \cos(q - q')), \end{aligned} \quad (\text{S9})$$

and annihilation of q' and q modes

$$\begin{aligned} f_{q',q}^a = & v_q^2 u_{q'}^2 (1 + \cos q') + u_q^2 v_{q'}^2 (1 + \cos q) \\ & - u_q v_q u_{q'} v_{q'} (1 + \cos q' + \cos q + \cos(q - q')). \end{aligned}$$

As written in the main text, Eq. (3), the update of Lagrange multipliers is related to the update of conserved quantities via susceptibility matrix, which is for occupation operators simply diagonal $\dot{\mu}_q(t) = -\frac{\langle \dot{n}_q \rangle(t)}{\chi_{q,q}(t)}$, $\chi_{q,q}(t) = \frac{e^{-\mu_q(t)}}{(1 + e^{-\mu_q(t)})^2}$.

Considered Lindblad dissipators preserve the particle number parity, Eq.(S6), therefore the dynamics in the two parity sectors is decoupled at the level of zeroth order approximation $\rho_\lambda(t)$. However, at finite coupling to

baths this symmetry is lost. When comparing the GGE results in the main text to finite coupling tensor network ones, we perform averaging over both parity sectors, which are indistinguishable in the thermodynamic limit anyway.

Frobenius distance for free fermion representation of density matrices

We outline the procedure for calculating the distance between reduced density matrices (RDMs) of two Gaussian states, used in the main text on the zeroth order $\rho_{\lambda}(t)$ approximation of dynamics, Eq. (2), for the integrable Hamiltonian.

Consider a subsystem of interest A consisting of the first ℓ spins, located on sites $i = 1, \dots, \ell$ and the reduced density matrix $\rho_A = \text{Tr}_A[\rho]$ of state ρ . It is convenient to represent ρ_A in terms of Majorana fermions:

$$\rho_A = \frac{1}{2^\ell} \sum_{\mu_i=0,1} \text{Tr} \left[\rho \prod_{i=1}^{2\ell} a_i^{\mu_i} \right] \left(\prod_{i=1}^{2\ell} a_i^{\mu_i} \right)^\dagger \quad (\text{S10})$$

where $a_{2i} = c_i + c_i^\dagger$, $a_{2i-1} = i(c_i - c_i^\dagger)$ and c_i is a fermionic operator as introduced in the previous section. Importantly, the reduced density matrix of a Gaussian state is also Gaussian. A central quantity that characterizes the reduced density matrix is the correlation matrix Γ , defined on subsystem A of length ℓ by:

$$\Gamma_{A,ij} = \text{Tr}[a_i a_j \rho] - \delta_{ij}, \quad 1 \leq i, j \leq 2\ell \quad (\text{S11})$$

Using Wick's theorem, the reduced density matrix can be expressed in Gaussian form

$$\rho_A \sim e^{-\frac{1}{4} a_i W_{A,ij} a_j}, \quad \text{where} \quad \tanh \left(\frac{W_A}{2} \right) = \Gamma_A \quad (\text{S12})$$

Given the correlation matrices, the trace of the product of RDMs can be computed using [102]:

$$\text{Tr}[\rho_A \tilde{\rho}_A] = \left(\det \left| \frac{1 + \Gamma_A \cdot \tilde{\Gamma}_A}{2} \right| \right)^{\frac{1}{2}}. \quad (\text{S13})$$

Thus, the Frobenius distance between two reduced density matrices is obtained from substituting Eq.(S13) into the expression

$$\text{Tr}[(\rho_A - \tilde{\rho}_A)^2] = \text{Tr}[\rho_A^2] + \text{Tr}[\tilde{\rho}_A^2] - 2\text{Tr}[\rho_A \tilde{\rho}_A] \quad (\text{S14})$$

We now turn from the discussion of distances from two general Gaussian density matrices to those given by the GGE (S4) of transverse field Ising model. In that case, the Majorana fermions operators can be linearly expressed in terms of Bogoliubov quasiparticle operators $d_q^\dagger d_p$, Eq. (S3), with simple expectation value

$$\text{Tr}[d_q^\dagger d_p \rho_{\lambda}] = \delta_{q,p} \frac{e^{-\mu_q}}{1 + e^{-\mu_q}}. \quad (\text{S15})$$

This simplifies the structure of the correlation matrix, which has the block-Toeplitz form

$$\Gamma_A = \begin{pmatrix} \Gamma^{(0)} & \Gamma^{(-1)} & \dots & \Gamma^{(1-\ell)} \\ \Gamma^{(1)} & \Gamma^{(0)} & \dots & \vdots \\ \vdots & \ddots & \ddots & \vdots \\ \Gamma^{(\ell-1)} & \dots & \dots & \Gamma^{(0)} \end{pmatrix}, \quad (\text{S16})$$

where

$$\Gamma^{(m)} = \frac{i}{L} \sum_k \tanh \frac{\mu_k}{2} \begin{pmatrix} 0 & g^{(m)}(k) \\ -g^{(m)}(-k) & 0 \end{pmatrix}, \quad (\text{S17})$$

and

$$\begin{aligned} g^{(m)}(k) = & (u_k^* v_k + u_k v_k^*) \sin(mk) - \\ & (|u_k|^2 - |v_k|^2) \cos(mk). \end{aligned} \quad (\text{S18})$$